Chapter 1

Introduction

This chapter gives a brief introduction to surfactants and polyelectrolytes and x-ray diffraction techniques. The phase behaviour of surfactant systems and the physical characteristics of polyelectrolytes have been discussed in sections 1.1 and 1.2 respectively. The mechanism which drives complex formation between oppositely charged surfactants and polyelectrolytes is described in section 1.3. The theory of x-ray diffraction and the characterization of the different liquid crystalline phases exhibited by surfactant solutions using diffraction methods have been outlined in section 1.4. Finally, the experimental set up, the method of sample preparation, the chemicals used and other experimental details are presented in section 1.5.

1.1 Surfactants

Amphiphilic molecules consist of long hydrocarbon chains covalently attached to molecular groups that tend to associate with water [1, 2]. The hydrocarbon chain is referred to as the tail of the amphiphile and the water-loving molecular group, as the head group. Synthetic amphiphiles are often referred to as surfactants, whereas those of biological origin are usually called lipids. Though this nomenclature is not standard, this is the sense in which these two terms are used here. Depending on the nature of the head group, amphiphiles can be classified as ionic, non-ionic and zwitter-ionic. Ionic amphiphiles dissociate in water and acquire an electric charge. Examples are the single-tailed surfactant cetyltrimethylammo-

nium bromide (CTAB) (fig.1.1A), the double-tailed didodecyldimethylammonium bromide (DDAB) (fig. 1.1B) and the cationic lipid dioleoyltrimethylammonium propane (DOTAP) (fig 1.2). Non-ionic amphiphiles like dodecylhexapolyethyleneoxide ($C_{12}E_6$) have polar head groups which are not charged. In the case of zwitterionic amphiphiles like dioleoylphosphatidyl choline (DOPC) (fig 1.3), the head group acquires a dipole moment in aqueous solutions.

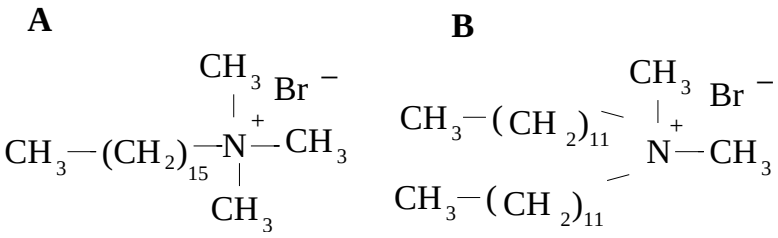

Figure 1.1: Structure of CTAB (A) and DDAB (B).

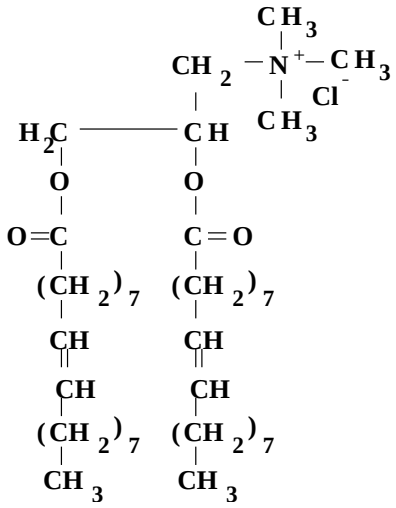

Figure 1.2: Structure of dioleoyltrimethylammonium propane (DOTAP).

1.1.1 The Hydrophobic effect

The interaction between water molecules involve orientation dependent hydrogen bonds with interaction energies in the range 3 - 5 k_BT, where k_B is the Boltzmann constant and T the temperature. At room temperature, each water molecule is on an average hydrogen bonded

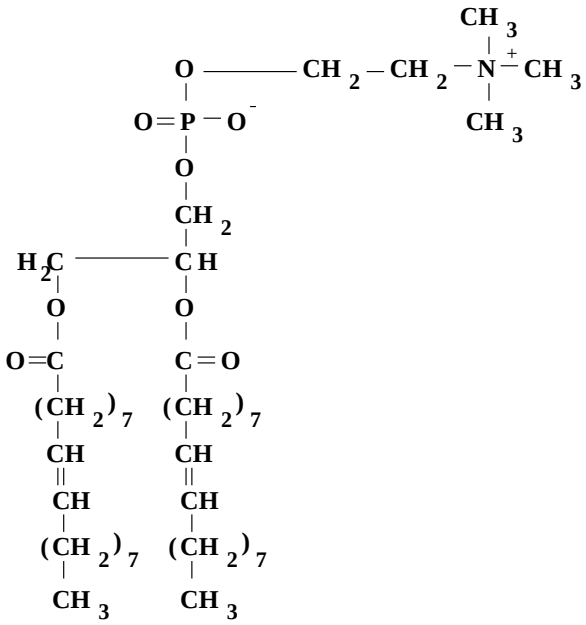

Figure 1.3: Structure of dioleoylphosphatidyl choline (DOPC).

to 3-3.5 molecules. The addition of nonpolar solute molecules like inert atoms, hydrocarbons and fluorocarbons in aqueous solutions disrupts the hydrogen bonds between the water molecules. The water molecules can however form a tetrahedral structure with each other and reorient themselves around these molecules to form 'cage-like' structures. Depending on the size of the solute molecules, they become more ordered than the molecules in the bulk liquid, resulting in a decrease in the entropy of the system. Hence it becomes thermodynamically unfavourable for nonpolar molecules like hydrocarbons to dissolve in water. This immiscibility of inert substances in water which is of entropic origin is known as the hydrophobic effect [2, 3].

1.1.2 Self assembly of amphiphiles

Amphiphilic molecules have low solubilities in water as a result of the hydrophobic effect. They form monolayers at air-water interface in order to minimize contact between their tails and water. Some amphiphiles can form aggregates called micelles in water, where the head groups shield the chains from coming in contact with water. This process is called self

assembly [1, 2].

From a thermodynamic point of view, an aqueous solution of an amphiphile can be considered as a multicomponent system with several phases in equilibrium. Each phase is taken to consist of aggregates of a given aggregration number, which is the number of molecules in an aggregate. For a very dilute solution, the interaction between the aggregates may be neglected and one can apply the theory of dilute solutions to this system.

The chemical potential of an amphiphile in an s-aggregate is given by

$\tilde{\mu_s} = \tilde{\mu_s^o} + (k_B T/s) ln(X_s/s)$

$\tilde{\mu_s^o}$ is the standard part of the chemical potential containing contributions from the interactions of the amphiphiles within the s-aggregate. The second term comes from the entropy of mixing. X_s is the mole fraction of amphiphiles that form s-aggregates. The total mole fracton of the amphiphiles X = $\sum_{s=1}^{\infty} X_s << 1$. In chemical equilibrium, the chemical potential of the amphiphile $\tilde{\mu_s}$ remains the same for all s. Thus

$$\tilde{\mu_1^o} + k_B T ln(X_1) = \tilde{\mu_2^o} + (k_B T/2) ln(X_2/2) = ...$$
$$= \tilde{\mu_n^o} + (k_B T/n) ln(X_n/n)$$

This gives the equilibrium distribution of the s-aggregates as

$X_s/s = X_1^s e^{s(\tilde{\mu_1^o} - \tilde{\mu_s^o})/k_B T}$

If we define $\alpha = (\tilde{\mu_1^o} - \tilde{\mu_s^o})/k_B T$, then $X_s = s(X_1 e^{\alpha})^s$.

Therefore, aggregation can take place only if $\alpha > 0$. Hence the energy per molecule must be lower in aggregates of size M, for some M > 1. In practice, M ~ 50, and is determined by the optimal packing of the hydrocarbon chains within the micelles.

Since X_s cannot exceed unity, the limiting value of monomer concentration, $X_1 \sim e^{-\alpha}$. The critical micellar concentration (CMC), is the amphiphile concentration at which X_1 saturates and further addition of amphiphiles leads to the formation of micelles (fig 1.4). It is given by, CMC $\approx e^{-\alpha}$

Hence larger the enthalpy gain in forming an aggregate, the lower the CMC. At CMC, many physical properties of the amphiphile solution exhibit an anomalous behaviour (fig

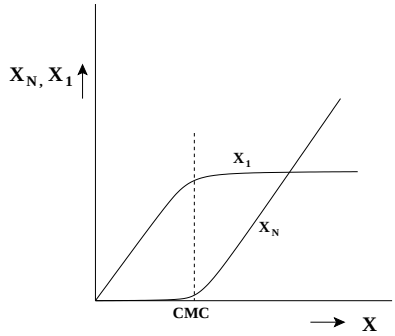

Figure 1.4: Variation of X_1 and X_N as a function of the amphiphile concentration X.

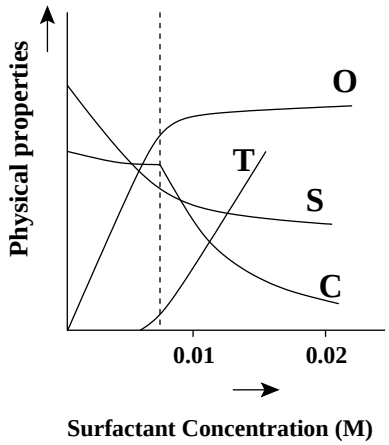

Figure 1.5: Effect of micellization on the bulk properties of surfactant solutions. O, T, S and C denotes the osmotic pressure, turbidity, surface tension and equivalent conductivity of the surfactant solution respectively. The dashed line indicates the critical micellar concentration (CMC). The CMC value and concentration scale corresponds to an aqueous solution of sodium dodecylsulphate. [4]

1.5). These trends can be used to estimate the CMC of an amphiphile in aqueous solution. For CTAB, CMC ~ 1 mM.

Just above CMC, the amphiphiles generally form spherical micelles (fig 1.6). At higher concentrations, they usually form disk-like or rod-like micelles. The size distribution of micelles depends on the aggregate geometry. Spherical micelles (fig 1.6), whose radius is determined by the alkyl chain length of the amphiphile, remain fairly monodisperse. Disk-like micelles whose thickness h $\approx$ 2l where l is the length of the hydrocarbon chain, form infinite bilayers, even at low surfactant concentration. Rod-like micelles whose radius r $\approx$ l are however found to be highly polydisperse. In order to prevent the hydrocarbon chains from

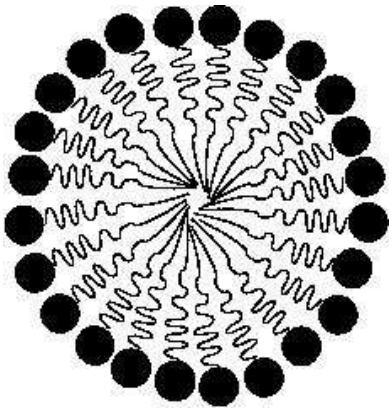

Figure 1.6: Schematic diagram of the crosssection of a spherical micelle, formed in dilute surfactant solutions above CMC.

being in contact with water, the disks have semitoroidal rims and the rods have hemispherical end caps. The formation of these curved edges, however cost energy. The difference in the behaviour of disc-like and rod-like micelles arises from the fact that the perimeter of the rim of a disk increases with the disk radius, whereas the size of the end cap on a cylinder is independent of the length of the cylinder.

If we neglect the inter-aggregate interactions, the average size of a rod-like micelle is given by

$< s >= 2(Xe^{\delta})^{1/2}$

X is the concentration of the amphiphile and δ the energy cost for creating an end cap. δ can be made very large by adding certain salts and alcohols to the amphiphile solution. This results in the formation of very long, flexible micelles that become entangled to form a viscoelastic gel. These are known as 'worm-like' micelles and behave in many ways similar to polymers [5].

1.1.3 Phase behaviour of surfactant solutions

Surfactant solutions exhibit many liquid crystalline phases at high surfactant concentrations. All these phases are characterized by long range orientational order of the aggregates.

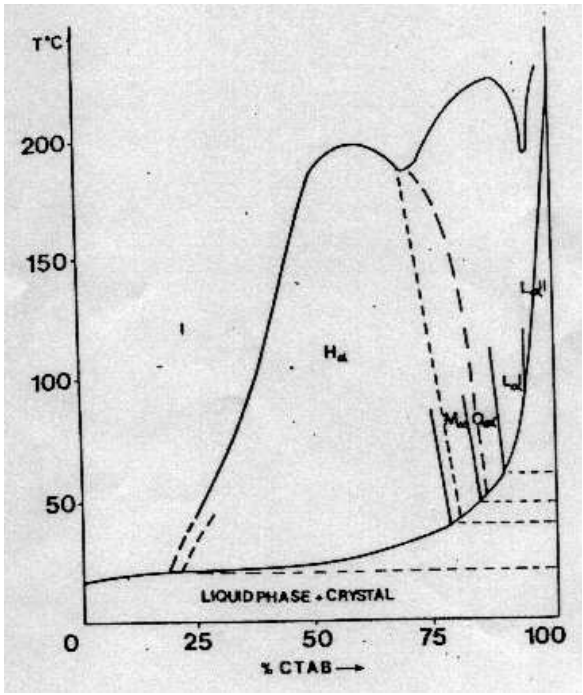

Figure 1.7: Partial temperature-composition phase diagram of CTAB-water system. I, H_α, M_α and Q_α denote the isotropic, 2D hexagonal, monoclinic and cubic phases. L_α^I denotes the lamellar phase obtained at lower temperatures where the bilayers are separated by water and L_α^{II} is the lamellar phase at high temperatures where the bilayers are collapsed with very little water between them [6].

Here we shall discuss the phase behaviour of two surfactant systems, one of which forms rod-like and the other disc-like aggregates in dilute solutions.

The phase diagram of CTAB-water system is given in figure 1.7 [6]. Just above CMC, the solution consists of spherical micelles. However they transform to rod-like micelles at a higher surfactant concentration (ϕ_s). The rods are randomly oriented and have no positional correlations. Hence the solution is isotropic.

On increasing ϕ_s, the length of the rods increases and long range positional and orientational order develop in the system, with cylindrical micelles arranging themselves on a 2D hexagonal lattice (fig 1.8). At 30^oC, hexagonal phase appears over a wide range of surfactant concentration in the CTAB-water system. When the surfactant content is higher than 75 %, a monoclinic phase (M_α) appears above 50^oC. This phase consists of long aggregates with an almost elliptical cross section, termed as 'ribbon-like', arranged on a 2D oblique lattice.

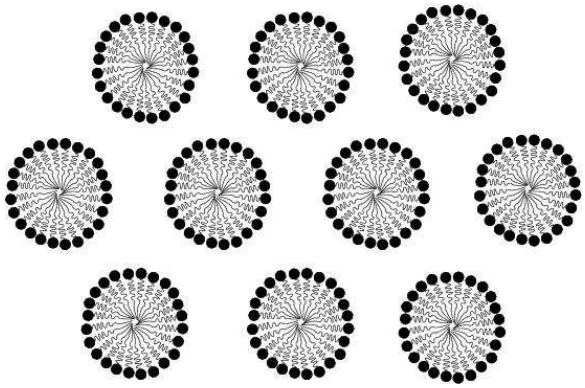

Figure 1.8: Schematic diagram of the hexagonal phase which consists of cylindrical micelles arranged on a 2D hexagonal lattice. The cylinders are oriented normal to the plane shown.

Figure 1.9: Schematic diagram of the lamellar phase which consists of bilayers stacked one above the other. d is the lamellar periodicity.

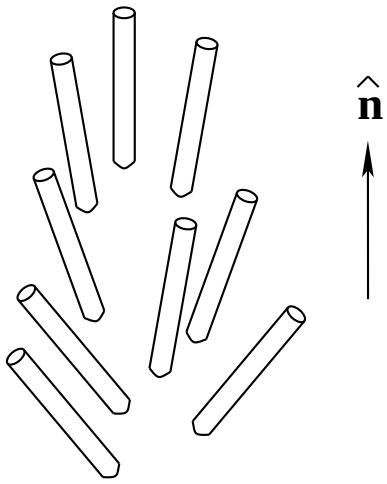

Figure 1.10: Schematic diagram of nematic phase formed by rod-like micelles. $\hat{\mathbf{n}}$ is the apolar director.

Beyond the monoclinic phase, a cubic phase (Q_α) appears. At very high ϕ_s, a lamellar phase is observed in the system which consists of bilayers separated by water (L_α^I) (fig 1.9). At high temperatures, above 80 ^oC another lamellar phase (L_α^{II}) is observed in which the bilayers are collapsed, with very little water between them. The reason for the formation of L_α^{II} is not known at present.

In some systems, in between the isotropic and hexagonal phases, the rod-like micelles acquire long range orientational order to form a nematic phase. This phase is also exhibited occasionally by disk-like micelles in between the isotropic and lamellar phases. Here the symmetry axis of the rod-like (disk-like) micelle has a preferred direction of orientation which is referred to as the nematic director $\hat{\mathbf{n}}$ (fig 1.10).

In the cesium pentadecaflourooctanoate (CsPFO)-water system (fig 1.11), the dilute solution consists of disk-like micelles [7]. At a higher surfactant concentration a nematic phase formed by disk-like micelles is obtained (N_D^+). Further increase in the concentration leads to the appearance of a lamellar phase (L_D). Transitions between these three phases can also be driven by changing the temperature at intermediate values of ϕ_s.

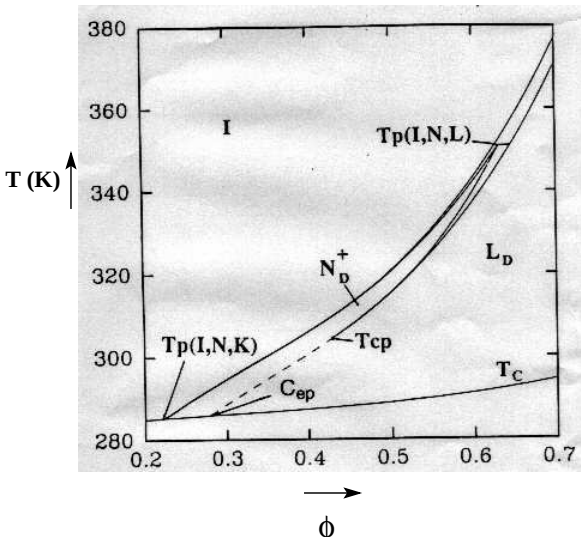

Figure 1.11: Partial temperature-composition phase diagram of CsPFO-water system. I, N_D^+, L_D denotes the isotropic, nematic and lamellar phases formed by disc-like micelles [7]. T_p denotes the triple points where three phases meet. T_{cp} is a tricritical point across which the nematic to lamellar transition goes from being first order to continuous.

1.2 Polymers

Polymers are obtained by the covalent bonding of a large number of repeat units called monomers [8, 9]. A simple example is polyethylene, whose structure can be represented as $(-CH_2-CH_2-)_N$. The number of repeat units N is called the degree of polymerization. In a homopolymer, like polyethylene, the repeat units are identical. Polymers in which the repeat units vary are known as copolymers or heteropolymers. For example, single stranded DNA is a heteropolymer with 4 different types of repeat units.

The persistence length l_p, of a polymer is a measure of its flexibility. It can be defined in terms of the orientational correlation length of the tangent vector $\hat{t}(s)$ of the polymer backbone; $<\hat{t}(s).\,\hat{t}(s+r)> \sim e^{-r/l_p}$. Here <. ..> denotes the thermal average, and r is the countour length between the two points. A section of chain shorter than the persistence length behaves like a stiff rod and sections of the chain separated by a distance much larger than the persistence length l_p bend independently of each other. The persistence length of polyethylene is about 1.5 nm and consists of 4 to 5 C-C bonds whereas the persistence length of double

stranded DNA is about 50 nm and consists of roughly 150 bp.

Due to the flexibility of the polymer, any polymer chain which is sufficiently long, forms a random coil in a good solvent. To estimate the size of an ideal polymer chain, it can be treated as a random walk where each step is independent of the previous one. If b is the step size, then the k th step is given by $\mathbf{a}_k = b\hat{a}_k$. As $\mathbf{R} = \sum_{k=1}^{N} \mathbf{a}_k$, the mean square end to end distance is given by, $<R^2> = \sum_{k=1}^{N} \sum_{l=1}^{N} <\mathbf{a}_k.\mathbf{a}_l>$. Since each step is independent and can be oriented in any direction, $<\mathbf{a}_k.\mathbf{a}_l> = 0$, for $k \neq l$. Hence

$$<R^2> = N.\ b^2$$

Thus the root mean square end to end distance of a long ideal chain, is proportional to $N^{\frac{1}{2}}$. However in the above estimation, we have not taken into account the fact that different segments of the chain cannot intersect each other. Thus effectively there is a short range repulsive interaction between the chain segments. By taking into account these excluded volume effects, it has been shown that $R \sim N^{\frac{3}{5}}$.

1.2.1 Polyelectrolytes

Polymers in which, the monomers dissociate in aqueous solutions to become charged by releasing their counter ions are known as polyelectrolytes [9]. Examples of polyelectrolyes are DNA and poly (acrylic acid) (PAA). Since the number of charged monomers is equal to the number of counter ions, the polymer solution as a whole is electrically neutral. If e is the charge of a monomer and ϵ, the dielectric constant of the solution, then the Coulomb interaction between two charged monomers separated by a distance r, is given by
$V(r) = (e^2/\ \epsilon\ r)\ e^{(-r/\lambda_D)}$, where λ_D is the Debye screening length. $\lambda_D = [\frac{\epsilon k_B T}{4\pi n e^2}]^{\frac{1}{2}}$ where e is the elementary charge and n is the concentration of counter ions or the ionic strength of the solution. In a dilute polyelectrolyte solution, the concentration of counter ions is very low and λ_D is very large. Hence due to the long range Coulomb repulsion between the monomers, the chain remains fully extended and the end to end distance $R \sim N$.

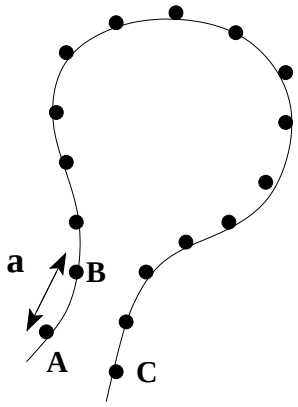

Figure 1.12: A polyelectrolyte chain which bends at length scales much larger than r_D.

In a polyelectrolyte solution of finite concentration, the presence of counter ions in the solution can screen the Coulomb interactions. Hence the polyelectrolyte no longer remains extended, but takes a coil-like configuration. However at shorter length scales, the polyelectrolyte remains stiff due to the electrostatic interactions. The persistence length of a polyelectrolyte (l_p) has contributions from the rigidity of the polymer backbone, known as the intrinsic persistence length (l_o), as well as from electrostatic interactions between the monomers (l_e). Electrostatic contributions can arise in two ways; At short length scales comparable to the separation between the charged monomers on the backbone $a << \lambda_D$, the Coulomb repulsion between the charges on the polymer backbone (A and B in fig 1.12), leads to the stiffening of the chain. At large length scales, when the chain bends, a Coulomb repulsion arises when the charges come closer (A and C in fig 1.12) than λ_D, which may also be classified under excluded volume interactions. Taking into account these interactions, the electrostatic contribution to the persistence length l_e is given by, $l_e = u\ \lambda_D^2/4a$, where $u = l_B/a$. $l_B = e^2/\epsilon k_B T$ is the Bjerrum length, k_B the Boltzmann constant and T the temperature. The Bjerrum length is the separation between two elementary charges at which the Coulomb interaction energy is $k_B T$. Typically, $u \sim 1$, $\lambda_D >> a$, when the salt concentration is not high. Therefore $l_e >> \lambda_D$. Hence the stiffening of the polymer chain due to electrostatic interaction occurs on length scales much larger than the Debye length.

1.2.2 Counter ion condensation

Besides screening the Coulomb interactions in the solution, the counter ions can also condense near the polymer chain in the case of highly charged polyelectrolytes, reducing the effective charge density. This is known as the Oosawa-Manning condensation [10]. The linear charge density $\rho_o = e/a$, where a is the separation between the charged units. In a salt free solution, some of the counter ions stay near the polymer and hence remain '*bound*', whereas the remaining can be anywhere in the solution and are $'free'$. In a simple treatment of the problem, these two regions may be considered as two phases coexisting in equilibrium and the condition under which the counter ions remain bound or condensed can be determined.

If c_1 and c_2 are the concentrations of bound and free counter ions in regions 1 and 2 respectively, and ψ_1 and ψ_2 the electrostatic potentials in these regions, $c_1 = c_2 e^{-e\delta\psi/k_BT}$, $\delta\psi = \psi_1 - \psi_2$. If β is the volume fraction of counter ions in region 2, and ϕ, the volume fraction of region 1 in the solution, then c_1 and c_2 can be expressed in terms of β and ϕ. Then the above relation becomes,

$\ln [(1-\beta)/\beta] - \ln [\phi/(1-\phi)] = -e\delta\psi/k_BT$

The polyelectrolyte can be represented as a cylinder at length scales $\sim \lambda_D$. Then the potential difference between regions 1 and 2 can be written as $\delta\psi = (-\rho/\epsilon)\ln(1/\phi)$. Since $(1-\beta)$ is the fraction of counter ions condensed, the effective charge density $\rho = e\,\beta/\,a$. In a dilute solution, $\phi << 1$. Hence

$ln[(1-\beta)/\beta] - \ln [\phi] = (-e^2\beta/\epsilon a k_BT) ln[\phi]$, or

$\ln[(1-\beta)/\beta] = (1-u\beta) \ln[\phi]$, where $u = (e^2/\epsilon a k_BT)$

Depending on the value of u, two different regimes of behaviour are found. If u <1, then as $\phi \rightarrow 0$, $\beta \rightarrow 1$, hence most of the counter ions remain in the solution. If u >1, then as $\phi \rightarrow 0$, $\beta \rightarrow 1/u$, and the fraction $(1-\beta)$ of the counter ions remain near the polyelectrolyte. This corresponds to counter ion condensation. For u <1, the effective charge density remains the same as the bare charge density. For u >1, the effective charge density is always less than

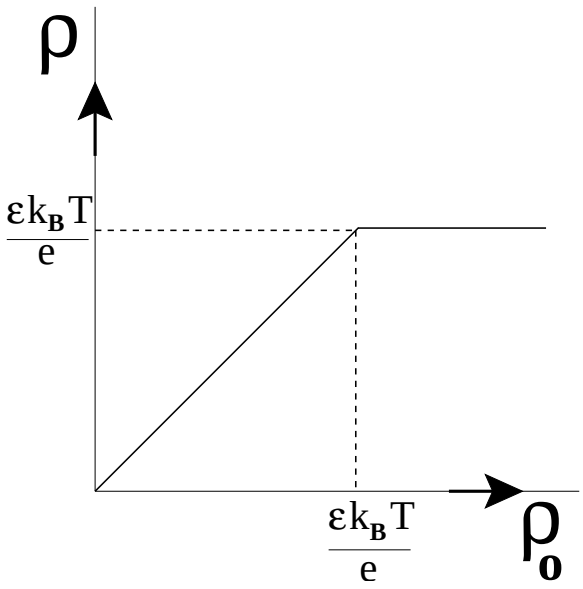

Figure 1.13: Dependence of the effective charge density (ρ) of the polyelectrolyte on the bare charge density (ρ_o). Counter ion condensation occurs for $\rho_o > \epsilon k_B T/e$, denoted by dashed line.

the bare charge density (fig 1.13). Since u = l_B/a, this means that the effective separation between the charges on the polyelectrolyte cannot be less than the Bjerrum length l_B.

Thus the phenomenon of counter ion condensation may be understood as follows: The electrostatic interaction of the counter ions with the polyelectrolyte $\sim 2\rho_o$ e lnr/ϵ, would restrict the counter ions to the vicinity of the polyelectrolyte segments. However this involves a loss in entropy of the counter ions $\sim k_B T lnr^2$. Since both the contributions are proportional to lnr, depending on the coefficient of lnr, the electrostatics or the entropy determines the counter ion distribution in the solution.

1.3 Formation of surfactant-polyelectrolyte complexes

Similar to the polyelectrolytes, the micelles of ionic surfactants also acquire a charge in aqueous solutions. Therefore, the counter ion condensation phenomenon discussed in the case of polyelectrolytes is also applicable here. However the extent of this condensation depends on the geometry of the aggregates. Poisson-Boltzmann theory shows that in pla-

nar bilayers, the counter ions remain always condensed independent of the surface charge density [11]. For a spherical micelle, however, the counter ions remain in solution. The behaviour in the case of long rod-like micelles is similar to that in polyelectrolytes.

In a dilute solution containing oppositely charged surfactants and polyions, the surfactant ion can associate with the polyion to release their corresponding condensed counter ions into the solution. The resultant increase in the entropy of the counter ions is the driving mechanism for complex formation between surfactants and polyelectrolytes. The complex phase separates out of the aqueous solution as a precipitate. Most of the counter ions remain in the aqueous solution which is known as the supernatant. This complex is birefringent and forms various liquid crystalline phases which are described in the subsequent chapters of this thesis.

Counter ion release has been experimentally verified in complexes of the cationic lipid dioleoyltrimethylammonium propane (DOTAP) with ds DNA [12]. The increase in electrical conductivity of the solution due to the counter ion release has been determined from conductivity measurements. It is found that the increase is maximum at the DNA concentration corresponding to the isoelectric point, where all the charges on the DNA can be neutralized by the cationic lipid.

1.4 Theory of x-ray diffraction

X-rays are transverse electromagnetic radiations of short wavelength. The diffraction of x-rays occur due to the scattering by the electrons in the material. The interference of these scattered waves gives rise to the observed diffraction pattern [13, 14]. Hence we consider only coherent, elastic scattering events.

Consider a plane wave of amplitude ϕ_o and wave vector $\mathbf{k}_o$, incident on two electrons,

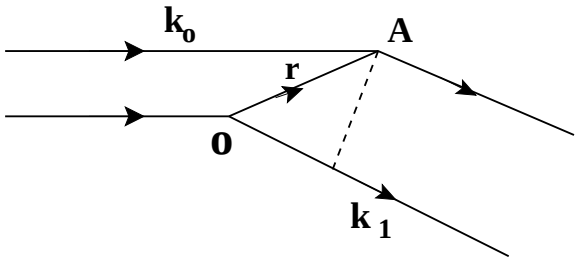

Figure 1.14: Scattering from discrete points; $\mathbf{k}_o$ and $\mathbf{k}_1$ denotes the incident and scattered wave vectors. O is the origin. A is a point at a distance **r** from the origin.

one of which is at the origin and the other at **r**

$\phi_{inc} = \phi_o e^{i\mathbf{k}_o.\mathbf{r}}$

The amplitude of the spherical wave scattered by the two electrons at a distance **R** (| **R** | >> | **r** |) is given by

$\phi_{sc} = (\phi_o a/\mathrm{R})\, e^{(ikR)}(1 + e^{i\mathbf{q}.\mathbf{r}})$

where a is the scattering length that determines the strength of scattering and $\mathbf{q} = \mathbf{k}_1 - \mathbf{k}_o$ is called the scattering vector. $q = |\mathbf{q}| = 4\pi sin\theta/\lambda$ is the scattering wave vector where λ is the wavelength of the incident wave and 2θ the scattering angle. $\mathbf{k}_1$ is the wave vector in the direction of **R**. Since we consider only elastic scattering, $|\mathbf{k}_o| = |\mathbf{k}_1| = k$. If we have an assembly of N electrons at positions $\mathbf{r}_i$, i = 1, 2, 3 ..., then

$\phi_{sc} = (\phi_o a/\mathrm{R}) \sum_{i=1}^{N} e^{i(kR - \mathbf{q}.\mathbf{r}_i)}$,

For a continuum distribution of electrons given by density $\rho(\mathbf{r}) = \sum_{i=1}^{N} \delta(\mathbf{r} - \mathbf{r}_i)$,

$$\phi_{sc} = (\phi_o a/R) e^{(ikR)} \int \rho(\mathbf{r}) e^{-i\mathbf{q}.\mathbf{r}} \mathbf{dr}$$

Thus the scattered amplitude is proportional to the Fourier transform of the electron density of the scattering medium. Here we assume that the scattering is sufficiently weak so that there is no reduction in the intensity as the incident wave propagates through the medium. Hence multiple scattering events are not considered.

The intensity of the scattered radiation $I(\mathbf{q}) = |\phi_{sc}|^2 R^2 / |\phi_{inc}|^2 = A|F(\mathbf{q})|^2$, where

$$F(\mathbf{q}) = \int \rho(\mathbf{r}) e^{-i\mathbf{q}.\mathbf{r}} \mathbf{dr}$$

A is a constant independent of q.

A periodic structure like a crystal consists of an arrangement of a repetitive unit called the basis on a lattice. Hence $\rho(\mathbf{r})$ of such a system can be described as the convolution of a function representing the lattice $\rho_L(\mathbf{r})$ with another function representing the basis $\rho_b(\mathbf{r})$ [14]. $\rho(\mathbf{r}) = \rho_L(\mathbf{r}) \otimes \rho_b(\mathbf{r})$.

The structure of the lattice may be described in terms of a set of delta functions, given by

$$\rho_L(\mathbf{r}) = \sum_m \sum_n \sum_p \delta(\mathbf{r} - m\mathbf{a} - n\mathbf{b} - p\mathbf{c})$$

where **a**, **b**, **c** are the basis vectors of the lattice. m, n, p are integers.

Taking the Fourier transform, we get

$F(\mathbf{q}) = F_L(\mathbf{q}).\ F_b(\mathbf{q})$ and hence $I(\mathbf{q}) = |F_L(\mathbf{q})|^2.\ |F_b(\mathbf{q})|^2$.

$F_L(\mathbf{q}) = \sum_h \sum_k \sum_l \delta(\mathbf{q} - h\mathbf{a}^* - k\mathbf{b}^* - l\mathbf{c}^*)]$ where **a***, **b***, **c*** are the basis vectors of the reciprocal lattice. h, k, l are integers.

$F(\mathbf{q})$ is often called the form factor of the basis and defined by

$$F_b(\mathbf{q}) = \int e^{-i\mathbf{q}.\mathbf{r}} \rho_b(\mathbf{r}) \mathbf{dr}$$

$F_b(\mathbf{q})$ gives the amplitude of the diffraction pattern sampled at the reciprocal lattice points determined by $F_L(\mathbf{q})$.

1.4.1 Polarization and geometric corrections

The scattered intensity from a sample is affected by certain factors that depend on the scattering angle. Therefore, the observed intensities have to be corrected for these effects be-

fore they can be put on a relative scale. The corrected scattered intensity is given by, I(**q**) = A p g I_o(**q**), where I_o(**q**) is the observed intensity and A, a constant independent of q. p and g depend on q and are called the polarization and geometric factors respectively.

The polarization factor, p = $(1 + cos^2 2\theta)^{-1}$, and arises from the fact that the the incident x-ray beam is unpolarized. In the case of small angle diffraction, $cos(\theta) \sim 1$ and hence this correction can be ignored.

The geometric corrrection, g, depends both on the type of sample and detector used in the experiment. In the case of unaligned samples, each diffraction peak is spread over a spherical shell of radius q. If a one dimensional detector is used to collect the data, then the observed intensity has to be multiplied by the area of this shell to get the total intensity of the peak; in this case $g = q^2$. On the other hand, if a two-dimensional detector like an image plate is used, rings obtained correspond to the intersection of these shells by a plane. If the observed intensities are integrated over these rings, then they have to be further multiplied by q to get the true intensities; in this case g = q.

1.4.2 Characterisation of liquid crystalline phases

The liquid crystalline phases are birefringent and exhibit characteristic textures when observed under a polarizing microscope. The typical textures of hexagonal and lamellar phases are shown in fig. 1.15 and fig 1.16 respectively. Since these mesophases have either long range or quasi long range positional order, x-ray diffraction gives sharp peaks in the small angle region.

The diffraction pattern of the lamellar phase is the easiest to identify. It consists of a set of peaks in the small angle region, the magnitude of their scattering vectors, q, being in the ratio 1:2:3 etc. These correspond to different orders of reflection from a lamellar periodicity d.

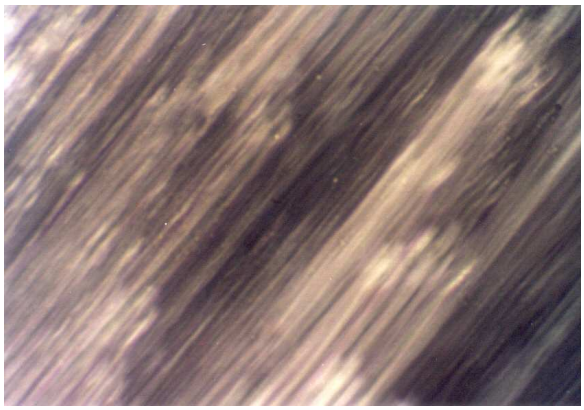

Figure 1.15: Typical texture of the hexagonal phase when observed between crossed polarizers.

The hexagonal phase gives rise to a set of peaks, whose q are in the ratio 1: $\sqrt{3}$: 2: $\sqrt{7}$: 3 etc. These correspond to the (1 0), (1 1), (2 0), (2 1) and (3 0) planes of a two dimensional hexagonal lattice. The lattice parameter is given by $a = 2\ d_{10}/\sqrt{3}$.

The lamellar and hexagonal phases can in general be identified unambiguously on the basis of their textures and diffraction patterns. However, this is not the case with the ribbon-phases. The textures exhibited by them are very similar to that of the hexagonal phase, as they are all characterized by a two-dimensional lattice. The diffraction patterns of these phases consist of a few peaks in the small angle region, with no specific relation between the corresponding values of q. In most of the cases these can be indexed on a centred rectangular lattice, such that reflections with h + k = odd integer, are absent. From the symmetry of the ribbons, these structures can be assigned to the plane group *cmm* (fig 1.17). Less frequently, the reflections can only be indexed on a rectangular *pgg* lattice, where (h 0) and (0 k) reflections with h and k odd are absent. In some rare cases the reflections cannot be indexed on a rectangular lattice, and an oblique lattice has to be invoked. Since the latter is the least symmetric one in two dimensions, all systems characterized by positional order in two dimensions can be indexed on such a lattice. In practice, we first try to fit a centred rectangular lattice, then rectangular, and finally an oblique lattice.

Figure 1.16: Typical texture of the lamellar phase when observed between crossed polarizers.

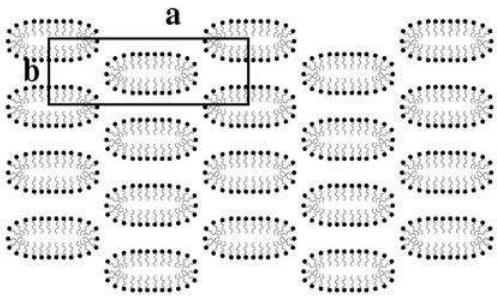

Figure 1.17: Schematic diagram of ribbon phase which consists of ribbon-like aggregates arranged on a 2D centred rectangular lattice. The long axis of the ribbons are normal to the plane shown.

1.5 Experimental Procedure

1.5.1 Experimental set up

X-rays were produced from a rotating anode x-ray generator (*Rigaku, UltraX* 18) operating at 50 kV and 80 mA. Cu K_α radiation of wavelength 0.154 nm was selected using a flat graphite monochromator (*Huber*). The sample taken in a glass capillary (*Hampton Research*, outer diameter - 0.5 to 1 mm, wall thickness - 0.01 mm) was placed in a locally built temperature controlled heater with a stability of ± 0.1 K. Most of the experiments were carried out at room temperature (30^{o}C). In a few cases, we have also carried out measurements at higher temperatures (up to 90 ^{o}C). The data were collected using an image plate (*Marresearch*, diameter 80 mm). The sample to film distance varied from 200 mm to 300 mm. Typical exposure times were one to 2 hours. The experimental set up is shown schematically in fig (1.18).

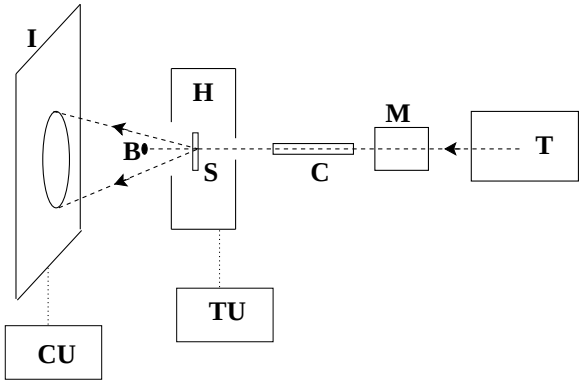

Figure 1.18: Schematic of the experimental set up. T, M, C, H, B, TU, I, CU, denotes the x-ray generator, monochromator, collimator, the heater, beamstop, temperature control unit, image plate and the scanning unit respectively. The dashed line represents the incident and scattered rays.

1.5.2 Sample preparation

Cetyltrimethylammonium bromide (CTAB)(fig 1 A), 3-hydroxy-2-naphthoic acid (HNA), didodecyldimethylammonium bromide (DDAB) (fig 1 B) and hexanol, were obtained from *Aldrich*. Sodium salts of calf thymus ds DNA (30 to 50 kbp) and poly (glutamic acid) (PGA) (fig 1.20) (MW=13650) were purchased from *Sigma*. M13 mp18 ss DNA (7250 bp) was ob-

tained from *Bangalore Genei*.

Poly (acrylic acid) (PAA) (fig 1.20) (MW=2000) and sodium salts of poly (vinyl sulfonate) (PVS) (fig 1.20) and poly (styrene sulfonate) (PSS) (MW=70000) (fig 1.20) were obtained from Aldrich. Sodium salt of PAA was prepared by adding equivalent amount of NaOH to water. 3-sodium-2-hydroxy naphthoate(SHN) (fig 1.19), was prepared by adding equivalent amounts of sodium hydroxide (NaOH) to the HNA solution. The bare charge densities and persistence lengths of the polyelectrolytes used are given in table 1.1.

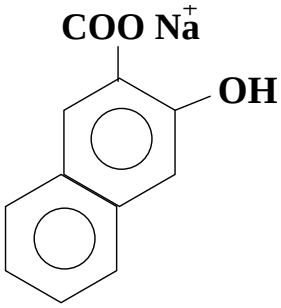

Figure 1.19: Structure of 3-sodium-2-hydroxy naphthoate (SHN).

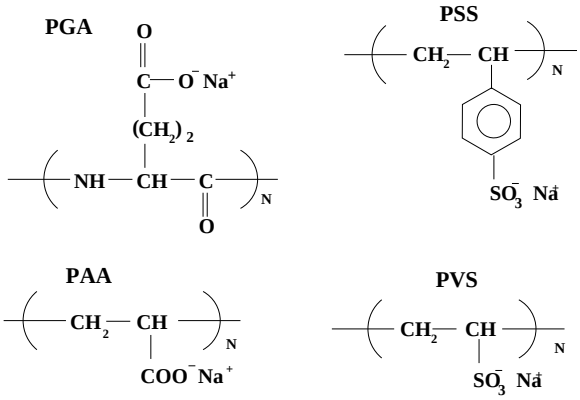

Figure 1.20: The structures of the polyelectrolytes used, namely, poly (glutamic acid) (PGA), poly (acrylic acid) (PAA), poly (vinyl sulfonate) (PVS), poly (styrene sulfonate) (PSS).

To prepare the complexes, surfactant solutions of appropriate concentrations were prepared using de-ionized water (Millipore). The polyelectrolytes were added to the solution. The complex which phase separates out was left in the solution for 3 or 4 days. It was then

Table 1.1: The bare charge densities and persistence lengths of the polyelectrolytes used namely double stranded (ds) DNA, single stranded (ss) DNA, poly (glutamic acid) (PGA), poly (acrylic acid) (PAA), poly (vinyl sulfonate) (PVS), poly (styrene sulfonate) (PSS).

Polyelectrolyte	bare charge density	l_p (nm)
ds DNA	1 $\overline{e}$/ 0.17 nm	50
ss DNA	1 $\overline{e}$/ 0.59 nm	1.5
PGA	1 $\overline{e}$/0.154 nm	2
PAA	1 $\overline{e}$/0.32 nm	1
PVS	1 $\overline{e}$/ 0.32 nm	1
PSS	1 $\overline{e}$/ 0.25 nm	10

transferred to a capillary along with some supernatant. The capillary was sealed using candle flame.

To prepare CTAB-SHN-water mixtures, appropriate amounts of CTAB and SHN were weighed out. The required concentration was obtained by adding the appropriate amount of water. The tubes containing the mixture were sealed and left in an oven at 40^{o}C, to equilibriate for about two weeks. For x-ray studies, the viscous samples were sucked into a glass capillary, flame sealed initially and later sealed with glue.

Bibliography

[1] W. M. Gelbart, A. Ben-shaul, D. Roux, Eds., *Micelles, Membranes, Microemulsions, and Monolayers* (Springer Verlag, New York, 1994)

[2] J. Israelachvili, *Intermolecular and Surface Forces*, 2nd edition (Academic Press, London, 1998)

[3] C. Tanford, *The Hydrophobic Effect*, 2nd edition (Wiley, New York, 1980).

[4] H. Wennerstrom and B. Lindman, Physics Reports **52**, 1 (1979).

[5] M. E. Cates and S. J. Candau, J. Phys. Condens. Matter **2**, 6869 (1990).

[6] X. Auvray, C. Petipas, R. Anthore, I. Ricco, and A. Lattes, J. Phys. Chem. **93**, 7458 (1989).

[7] N. Boden, K. W. Jolley, and M. H. Smith, Liq. Cryst. **6**, 481 (1989)

[8] G. Strobl, *The Physics of Polymers*, 2nd edition, (Springer Verlag, Berlin, 1997)

[9] A. Y. Grosberg and A. R. Khokhlov, *Statistical Physics of Macromolecules* (AIP Press, New York, 1994)

[10] F. Oosawa, Biopolymers **6**, 1633 (1968); G. S. Manning, J. Chem. Phys. **51**, 924 (1969).

[11] I. Rouzina, V. A. Bloomfield, J. Phys. Chem. **100**, 9977 (1996).

[12] K. Wagner, D. Harries, S. May, V. Kahl, J. O. Raedler, and A. Benshaul, Langmuir **16**, 303 (2000).

[13] D. C. Champeney, *Fourier Transforms and their Physical Applications*, (Academic Press, London, 1973).

[14] D. Sherwood, *Crystals, X – rays and Proteins*, Longman, 1976.